JPE 18-5-15

https://doi.org/10.6113/JPE.2018.18.5.1458
ISSN(Print): 1598-2092 / ISSN(Online): 2093-4718

Novel Model Predictive Control Method to Eliminate Common-mode Voltage for Three-level T-type Inverters Considering Dead-time Effects

Xiaodong Wang[*,**], Jianxiao Zou[†], Zhenhua Dong[*], Chuan Xie[*], Kai Li[*], and Josep M. Guerrero[***]

[†,*]School of Automation Engineering, University of Electronic Science and Technology of China, Chengdu, China
[**]Institute of Materials, China Academy of Engineering Physics, Mianyang, China
[***]Department of Energy Technology, Aalborg University, Aalborg, Denmark

Abstract

This paper proposes a novel common-mode voltage (CMV) elimination (CMV-EL) method based on model predictive control (MPC) to eliminate CMV for three-level T-type inverters (3LT2Is). In the proposed MPC method, only six medium and one zero voltage vectors (VVs) (6MV1Z) that generate zero CMV are considered as candidates to perform the MPC. Moreover, the influence of dead-time effects on the CMV of the MPC-based 6MV1Z method is investigated, and the candidate VVs are redesigned by pre-excluding the VVs that will cause CMV fluctuations during the dead time from 6MV1Z. Only three or five VVs are included to perform optimization in every control period, which can significantly reduce the computational complexity. Thus, a small control period can be implemented in the practical applications to achieve improved grid current performance. With the proposed CMV-EL method, the CMV of the $3LT^2Is$ can be effectively eliminated. In addition, the proposed CMV-EL method can balance the neutral point potentials (NPPs) and yield satisfactory performance for grid current tracking in steady and dynamic states. Simulation and experimental results are presented to verify the effectiveness of the proposed method.

Key words: Common-mode voltage, Model predictive control, Neutral point potentials, Three-level T-type inverters

I. INTRODUCTION

Three-level T-type inverters ($3LT^2Is$) are widely used for high-power, medium-voltage power conversion and drives [1]-[3] because they basically combine the advantages of the two-level inverters (such as low conduction loss, few devices, and simple operating principle) with the positive aspects of three-level inverters (such as low switching losses and superior output voltage quality) [4].

Traditional proportional-integral (PI) control with a pulse width modulation (PWM) block is most commonly used for inverters to provide output currents with controllable amplitude and frequency [5]-[8]. However, high common-mode voltages (CMVs) are generated by fast switching operation and dead-time effects [9]-[11]. The existence of high CMVs leads to serious problems, such as overvoltage stress to the winding of a motor and leakage currents in photovoltaic systems [12]-[15]. Therefore, various CMV reduction strategies on the basis of PWM techniques have been proposed in [14] [16]-[20]. However, all of these strategies require a complicated PWM modulator, which may cause conflicts between the elimination of CMV and the load current tracking control.

The model predictive control (MPC) is an optimization control scheme that is suitable for inverters because of its simplicity, fast dynamic response, and flexible constraint settings [11]. The reduction of CMV has been widely investigated using MPC method for two-level inverters [21]-[25]. These methods are mainly designed to avoid the utilization of zero voltage vectors (VV) to restrict the CMV within $\pm U_{dc}/6$. However, this technique is complicated for

Manuscript received Jan. 10, 2018; accepted May 3, 2018
Recommended for publication by Associate Editor Xiaoqiang Guo.
[†]Corresponding Author: jxzou@uestc.edu.cn
Tel: +86-17721888097, Univ. of Electronic Science and Tech. of China
[*]School of Automation Engineering, University of Electronic Science and Technology of China, China
[**]Institute of Materials, China Academy of Engineering Physics, China
[***]Department of Energy Technology, Aalborg University, Denmark

three-level inverters because of the increasing number of VVs. Furthermore, the problem of neutral point potential (NPP) unbalance exists for three-level inverters. In [26], a MPC-based method is proposed for 3LT^{2}Is to reduce the CMV and balance the NPPs. However, dead-time effects are not considered, and the CMV cannot be totally eliminated. A modified finite control set model predictive control (FCS-MPC) based method is proposed in [27] to reduce CMV fluctuations by adding additional terms to the cost function. This method is easy to understand. However, additional terms added to the cost function inevitably complicate the design of the weighting factors and increase the computational burden. Furthermore, dead-time effects are not considered, which may challenge the effectiveness and accuracy of the method.

This paper is an extended version of [28] with detailed analysis of dead-time effects on the CMV and sufficient performance comparison analysis. Based on [28], this paper presents a novel MPC-based method that considers dead-time effects to eliminate the CMV for 3LT^{2}Is. In the proposed MPC method, only six medium and one zero VVs (6MV1Z), which generate zero CMV, are considered candidates to perform MPC and eliminate CMV. The influence of dead-time effects on the CMV of the MPC-based 6MV1Z method is further analyzed, and a novel CMV elimination (CMV-EL) method is proposed on the basis of 6MV1Z method. In the proposed CMV-EL method, the VVs that will cause CMV fluctuations during the dead time are pre-excluded. As a result, only three or five VVs from 6MV1Z that will not cause CMV fluctuations during the dead time are utilized for optimization in every control period. Moreover, the three or five VVs used in CMV-EL method for CMV elimination can balance the NPPs and achieve satisfactory performance for grid current tracking in steady states and dynamic process. The calculation efforts will be significantly reduced if less VVs are utilized. Thus, a smaller control period can be implemented to achieve a better grid current performance. Both simulation and experimental results are included to verify that the proposed CMV-EL method can achieve a satisfactory performance in CMV elimination as well as grid current tracking and NPP balance control.

II. Conventional MPC Scheme for 3LT^{2}Is

The structure of the studied 3LT^{2}I is shown in Fig. 1. Each phase of the 3LT^{2}I is composed of four insulated gate bipolar transistor (IGBT) power switches with two of them connected to the neutral point O of the DC bus. This configuration allows the generation of three voltage levels at the output terminal of each phase with respect to the neutral point O, considering the switching function combinations $S_{x1}S_{x2}S_{x3}S_{x4}$ ($x = A, B, C$) expressed in Table I.

As shown in Table I, S_x and u_{xO} denote the switching variable and the output voltage of phase x, respectively. The

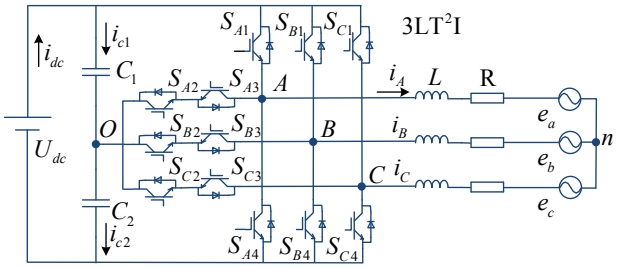

Fig. 1. Structure of the studied 3LT^{2}I.

TABLE I
Definition of Switching Variable

S_x	$S_{x1}S_{x2}S_{x3}S_{x4}$	u_{xO}	State
1	1 1 0 0	$U_{dc}/2$	P
0	0 1 1 0	0	O
−1	0 0 1 1	$-U_{dc}/2$	N

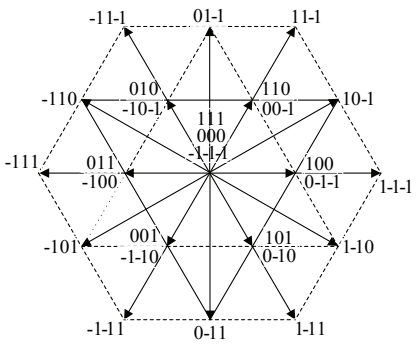

Fig. 2. Space vector diagram of the 3LT^{2}I.

switching functions of the IGBT take on the binary values 1 and 0 in a closed state and an open state, respectively. The output VV of the 3LT^{2}I can be described as

$$v = \frac{2}{3}\left(u_{AO} + u_{BO}e^{j(2\pi/3)} + u_{CO}e^{j(-2\pi/3)}\right). \quad (1)$$

Twenty-seven switching states exist for 3LT^{2}I, corresponding to six long vectors, six medium vectors, six small vectors, and one zero vector. Both zero and small vectors have redundant switching states. The relationship between the switching states and the VVs is shown in Fig. 2.

We assume that the bus voltage and the inductor currents are constant in a sampling interval and ignore the influence of dead time to simplify the explanation. The average model of the 3LT^{2}I in a two-phase stationary coordinate is expressed as

$$\begin{bmatrix} i_\alpha(k+1) \\ i_\beta(k+1) \end{bmatrix} = A\begin{bmatrix} i_\alpha(k) \\ i_\beta(k) \end{bmatrix} + B\begin{bmatrix} u_\alpha(k) - e_\alpha(k) \\ u_\beta(k) - e_\beta(k) \end{bmatrix}, \quad (2)$$

where $i_\alpha(k)$, $i_\beta(k)$, $u_\alpha(k)$, $u_\beta(k)$, $e_\alpha(k)$, and $i_\beta(k)$ are the grid current, output voltage, and grid voltage components of 3LT^{2}I in a two-phase stationary coordinate at instant k, $i_\alpha(k+1)$ and $i_\beta(k+1)$ are the predicted grid current at instant $k+1$, and A and B are shown as

$$A=\begin{bmatrix}1-RT_s/L & 0\\ 0 & 1-RT_s/L\end{bmatrix},\quad B=\begin{bmatrix}T_s/L & 0\\ 0 & T_s/L\end{bmatrix} \tag{3}$$

where T_s is the control period.

The dynamics of the DC link capacitor voltage is described by the differential equation shown as

$$\frac{dV_{cj}}{dt}=\frac{1}{C}i_{cj}, \tag{4}$$

where V_{cj} (j = 1,2) represents the voltage of the DC link capacitor, and C denotes the capacitor value. The capacitor voltage derivative dV_{cj}/dt is replaced by the forward Euler approximation expressed as

$$\frac{dV_{cj}}{dt}=\frac{V_{cj}(k+1)-V_{cj}(k)}{T_s}, \tag{5}$$

giving the discrete form of the DC link capacitor voltage shown as

$$V_{cj}(k+1)=V_{cj}(k)+\frac{1}{C}i_{cj}(k)T_s, \tag{6}$$

where current i_{cj} (k) depends on the switching states, and the grid currents of the 3LT^{2}I can be calculated using the following expression:

$$i_{cj}(k)=i_{dc}(k)-\sum_{x=A,B,C}H_{xj}i_x(k), \tag{7}$$

where i_{dc} is the current of the DC bus. The variable H_{jx} depends on the switching variable and is defined as

$$H_{xj}=\begin{cases}1 & \text{if}\,(S_x=1\,\&\,j=1)\,\text{or}\,(S_x=-1\,\&\,j=2)\\ 0 & \text{otherwise}\end{cases}. \tag{8}$$

To track the reference currents and balance the NPPs of the 3LT^{2}I, the cost function in conventional MPC for the 3LT^{2}I is expressed as [29]

$$\begin{aligned}g=&\left|i_\alpha^*(k)-i_\alpha(k+1)\right|+\left|i_\beta^*(k)-i_\beta(k+1)\right|\\&+\lambda_{dc}\left|V_{c1}(k+1)-V_{c2}(k+1)\right|\end{aligned}, \tag{9}$$

where $i^*_\alpha(k)$ and $i^*_\beta(k)$ are the reference currents at the instant k. The weighting factor λ_{dc} handles the relation between terms dedicated to reference current tracking and NPP balance. A larger value of λ_{dc} implies greater priority to the objective of NPP balance.

However, the unavoidable calculation delay in digital implementation has a significant influence on the performance of the 3LT^{2}I. To compensate the calculation delay in digital control [30], the cost function considers the current errors and difference of the DC link capacitor voltages at instant k + 2, which is expressed as

$$\begin{aligned}g=&\left|i_\alpha^*(k)-i_\alpha(k+2)\right|+\left|i_\beta^*(k)-i_\beta(k+2)\right|\\&+\lambda_{dc}\left|V_{c1}(k+2)-V_{c2}(k+2)\right|\end{aligned}, \tag{10}$$

TABLE II
RELATIONSHIP BETWEEN THE SWITCHING STATES AND CMV

Switching states ($S_AS_BS_C$)	CMV	Group
111	$U_{dc}/2$	*G1*
110, 011, 101	$U_{dc}/3$	*G2*
100, 010, 001, 11−1, −111, 1−11	$U_{dc}/6$	*G3*
000, 10−1, 01−1, −110, −101, 0−11, 1−10	*0*	*G4*
00−1, −100, 0−10, 1−1−1, −11−1, −1−11	$-U_{dc}/6$	*G5*
0−1−1, −10−1, −1−10	$-U_{dc}/3$	*G6*
−1−1−1	$-U_{dc}/2$	*G7*

where the predicted currents $i_\alpha(k+2)$ and $i_\beta(k+2)$ and the predicted voltages $V_{c1}(k+2)$ and $V_{c2}(k+2)$ are obtained by shifting the predicted values at instant $k+1$ one-step forward.

According to the aforementioned analysis, the future values of the grid currents and DC link capacitor voltages are predicted for all the 27 switching states. After obtaining the predictions, the cost function is evaluated for each switching state, and the one that minimizes the cost function is selected and applied during the next control period. However, adopting all the 27 switching states to perform the optimization in every control period will lead to considerable number of calculations, which have been demonstrated to be one of the main drawbacks of conventional MPC method for three-level inverters.

III. ANALYSIS OF CMV FOR 3LT^{2}IS CONSIDERING DEAD-TIME EFFECTS

The CMV of the 3LT^{2}I shown in Fig. 1, defined as the potential between the grid neutral point n and the neutral point of the DC bus, can be expressed with the pole voltages with respect to the neutral point of the DC bus as [17]

$$u_{\text{cmv}}=\frac{u_{AO}+u_{BO}+u_{CO}}{3}. \tag{11}$$

In the practical application, the potential of the neural point always needs to be controlled at approximately half of the DC bus voltage ($U_{dc}/2$) to achieve good performances of output waveforms. In this study, both voltages of positive and negative DC bus capacitor are directly assumed to be $U_{dc}/2$. Thus, the 3LT^{2}I takes the leg voltages on the discrete voltage levels with $\pm U_{dc}/2$ and an extra 0 compared with two-level inverters. According to Equation (10), the CMV generated by the 3LT^{2}I becomes $\pm U_{dc}/2$, $\pm U_{dc}/3$, $\pm U_{dc}/6$, and 0. Therefore, the 27 switching states are divided into seven groups by different CMV values in Table II, where the relationships between the switching states and CMV are summarized.

According to Table II, the large CMV fluctuations will be generated by the conventional MPC method for 3LT^{2}I because all the 27 switching states are utilized to perform the optimization during every control period. Moreover, although all the 27 switching states are utilized to perform the

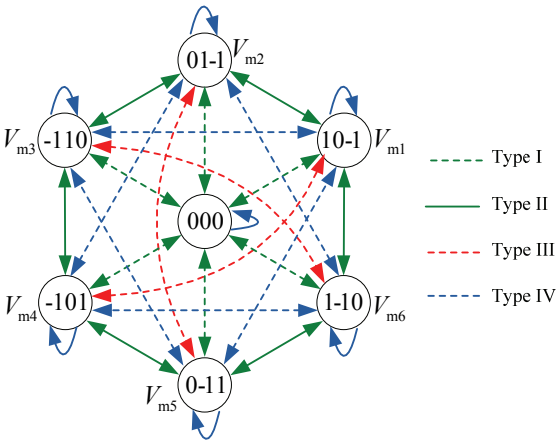

Fig. 3. Switch state graph of the 6MV1Z method.

optimization in every control period with the modified FCS-MPC method [26], only limited switching states that generate the same CMV are applied to the three-level inverter if the CMV is controlled as a constant value. Thus, to eliminate the CMV fluctuations with the reduced computational burden and design complexity, only the seven switching states from *G4* that correspond to six medium vectors and 1 zero vector (6MV1Z) that generate zero CMV are considered as candidates to perform the optimization in this study. Therefore, the CMV of 3LT^{2}I can be theoretically limited to zero if only VVs from 6MV1Z are utilized to perform the optimization in every control period. The switch state graph of the MPC-based 6MV1Z method is shown in Fig. 3.

As shown in Fig. 3, any VV is permitted to be applied in the next control period with the MPC method that is different from the conventional SVPWM method. The switching transitions of each VV from 6MV1Z include state transitions between state P and state O (PO), state O and state N (ON), and state P and state N (PN). An extra state transition PN is generated and compared with the PWM method.

However, because semiconductor devices are not ideal switches, the dead time is inevitably needed in practical application to prevent the disastrous shoot-through faults. During dead time, new states will be generated, which may cause large CMV fluctuations. Therefore, the influence of dead-time effects on the CMV when using the MPC-based 6MV1Z method will be analyzed first in this study. Considering the 3LT^{2}I leg of phase *x* shown in Fig. 4, the current flow paths of the state transitions PO, ON and PN during the dead time are shown in Fig. 4(a), (b), and (c), respectively, and DT1, DT2, and DT3 represent the corresponding states during the dead time.

As shown in Fig. 4, during the dead time, the uncontrollable grid current flows through the freewheeling diode, and the output voltage of each phase depends on the polarities of the current. The relationships between the output voltage and the polarities of the grid current for the states during dead time are summarized in Table III. During the

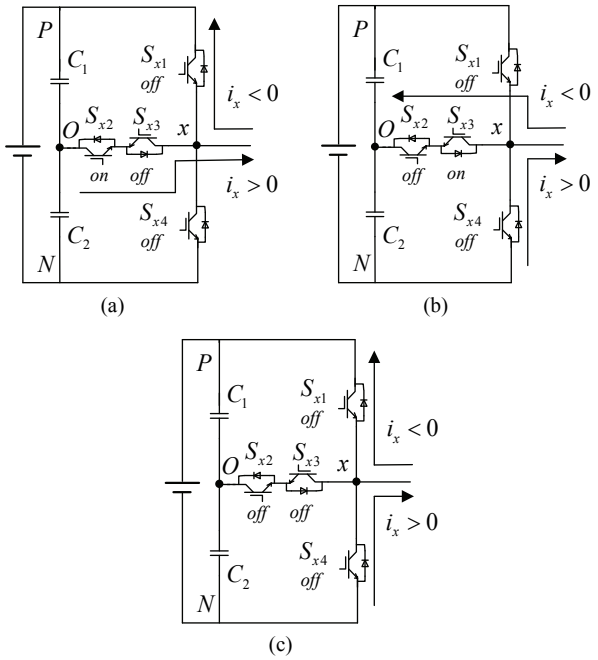

Fig. 4. Current flow paths of state transition during the dead time: (a) DT1(PO), (b) DT2(ON), (c) DT3(PN).

TABLE III
RELATIONSHIP BETWEEN OUTPUT VOLTAGE AND THE POLARITIES OF THE GRID CURRENT

State	Output voltage u_{xO}	
	$I_x>0$	$I_x<0$
DT1(0,1,0,0)	0	$U_{dc}/2$
DT2(0,0,1,0)	$-U_{dc}/2$	0
DT3(0,0,0,0)	$-U_{dc}/2$	$U_{dc}/2$

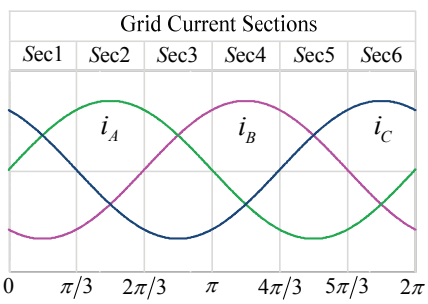

Fig. 5. Classification of one fundamental period of the grid currents.

dead time, the output voltage of each phase differs from different polarities of the grid current, which may cause large CMV fluctuations. Considering a balanced three-phase system, one fundamental period of the grid currents can be classified into six sections in which none of the grid currents change their polarities, as shown in Fig. 5.

The switching transitions which may cause CMV fluctuations during the dead time are divided into four different types to analyze the influence of dead-time effects of the VV switching transition on the CMV. The transitions

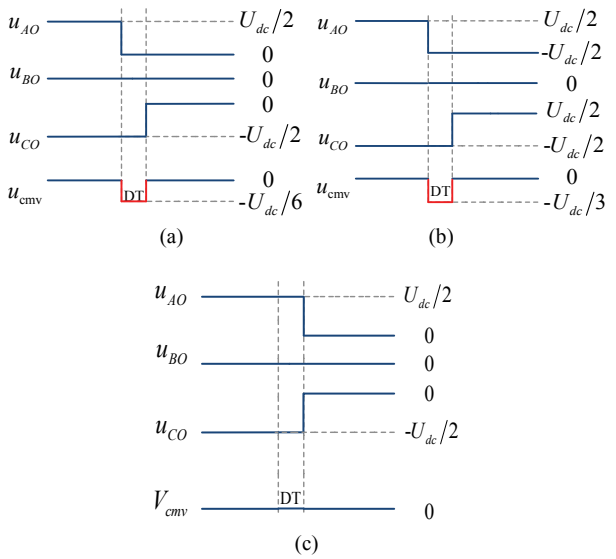

Fig. 6. Examples of switching transitions where two legs are involved: (a) Type I in *sec 1*, (b) Type III in *sec 1*, (c) Type II in *sec 2*.

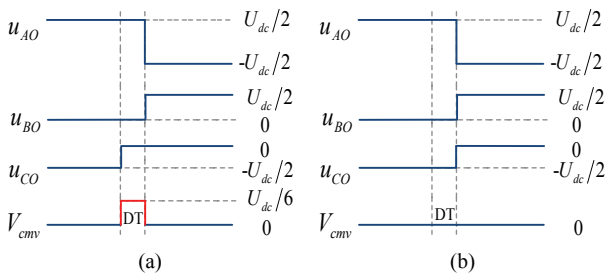

Fig. 7. Examples of switching transitions where three legs are involved: (a) Type IV in *sec 4*, (b) Type IV in *sec 5*.

are between nonzero VV and zero VV (Type I), nonzero VV and its adjacent VVs (Type II), nonzero VV and its opposite VV (Type III), and nonzero VV and its nonadjacent VVs (Type IV). The first three types of the VV switching transition involve two legs of the 3LT^{2}I, and the fourth one leads to the simultaneous commutations in three legs.

In reference to the case where two legs of the 3LT^{2}I are involved in the switching transition, for the switching transition of Type I, the two operational legs correspond to state transitions PO and ON. Meanwhile, for the switching transition of Type II, only state transition PO or ON is included, and only state transition PN is included for the switching transition of Type III. According to Table III, in reference to the case where two legs of the 3LT^{2}I are involved in the switching transition, the CMV of the 3LT^{2}I remains zero during the dead time if the grid currents of the operation legs are of different polarities. However, the same polarity of the output currents for the operation legs results in $\pm U_{dc}/6$ unplanned CMV fluctuations for the switching transition of Types I and II and $\pm U_{dc}/3$ CMV fluctuations for the switching transition of Type III during the dead time. Fig. 6 shows examples of the switching transition where two legs of the 3LT^{2}I are involved.

Similarly, for the switching transition of Type IV where three legs of the 3LT^{2}I are involved in the switching transition, the three operation legs correspond to state transitions PO, ON, and PN. According to Table III, the CMV of the 3LT^{2}I remains zero during the dead time if the grid currents of the two operation legs which correspond to state transitions PO and ON are with the same polarity. Otherwise, $\pm U_{dc}/6$ unplanned CMV fluctuations are generated for the switching transition of Type IV. Examples of the switching transition where three legs of the 3LT^{2}I are involved are shown in Fig. 7.

IV. Proposed Method for CMV Elimination Considering Dead-time Effects

The previous analysis of dead-time effects on the CMV of the switching transition between different VVs from 6MV1Z shows that CMV fluctuations may be generated during the dead time. In this study, a new MPC-based method is proposed on the basis of the 6MV1Z method to eliminate the CMV fluctuations during dead time. The candidate VVs for the proposed CMV elimination (CMV-EL) method are redesigned by pre-excluding the VVs that will cause CMV fluctuations during the dead time. As a result, only three or five VVs from 6MV1Z that will not cause CMV fluctuations during the dead time are utilized to perform the optimization in every control period. The candidate VVs for the proposed CMV-EL method are from different sections and are summarized in Table IV.

Take V_0 as the current VV in *sec 3* as an example. In the 6MV1Z method, if V_0 is applied in the current control period, all of the seven VVs from 6MV1Z are permitted to be applied in the next control period. However, if V_{m3} is chosen to be applied in the next control period, $-U_{dc}/6$ CMV fluctuation will be generated during the dead time. Meanwhile, in the proposed CMV-EL method, if V_0 is applied in the current control period, only V_0, V_{m1}, V_{m2}, V_{m4}, and V_{m5} are permitted to be applied in the next control period, which will not cause CMV fluctuations during the dead time. However, it should be noted that the proposed CMV-EL method can only be applied with the maximum amplitude of the phase-to-neutral voltages equal to $U_{dc}/2$, resulting in 86.6% of the voltages that can be obtained with the SVPWM and the conventional FCS-MPC method.

As shown in Table IV, the candidate VVs are the same for *sec 1* and *sec 2*, *sec 3* and *sec 4*, and *sec 5* and *sec 6*. The switch state graphs of the proposed CMV-EL method are shown in Fig. 8.

Controlling the use VVs from 6MV1Z is the best choice to maintain the CMV constant zero, but these VVs may cause NPP imbalance. The equivalent circuits when V_0 and V_{m1} is applied to 3LT^{2}I are shown in Fig. 9(a) and (b), respectively. i_O represents the current flow through the neutral point of the dc bus. i_O equals 0 and i_B for a balanced three-phase system

TABLE IV
CANDIDATE VVS FOR THE PROPOSED CMV-EL STRATEGY

VV	*Candidate VV combinations*		
	Sec 1 & sec 4	*Sec 2 & sec 5*	*Sec 3 & sec 6*
V_0	$V_0V_{m2}V_{m3}V_{m5}V_{m6}$	$V_0V_{m1}V_{m3}V_{m4}V_{m6}$	$V_0V_{m1}V_{m2}V_{m4}V_{m5}$
V_{m1}	$V_{m1}V_{m2}V_{m6}$	$V_0V_{m1}V_{m2}V_{m3}V_{m4}$	$V_0V_{m1}V_{m4}V_{m5}V_{m6}$
V_{m2}	$V_0V_{m1}V_{m2}V_{m5}V_{m6}$	$V_{m1}V_{m2}V_{m3}$	$V_0V_{m2}V_{m3}V_{m4}V_{m5}$
V_{m3}	$V_0V_{m3}V_{m4}V_{m5}V_{m6}$	$V_0V_{m1}V_{m2}V_{m3}V_{m6}$	$V_{m2}V_{m3}V_{m4}$
V_{m4}	$V_{m3}V_{m4}V_{m5}$	$V_0V_{m1}V_{m4}V_{m5}V_{m6}$	$V_0V_{m1}V_{m2}V_{m3}V_{m4}$
V_{m5}	$V_0V_{m2}V_{m3}V_{m4}V_{m5}$	$V_{m4}V_{m5}V_{m6}$	$V_0V_{m1}V_{m2}\ V_{m5}V_{m6}$
V_{m6}	$V_0V_{m1}V_{m2}V_{m3}V_{m6}$	$V_0V_{m3}V_{m4}V_{m5}V_{m6}$	$V_{m1}V_{m5}V_{m6}$

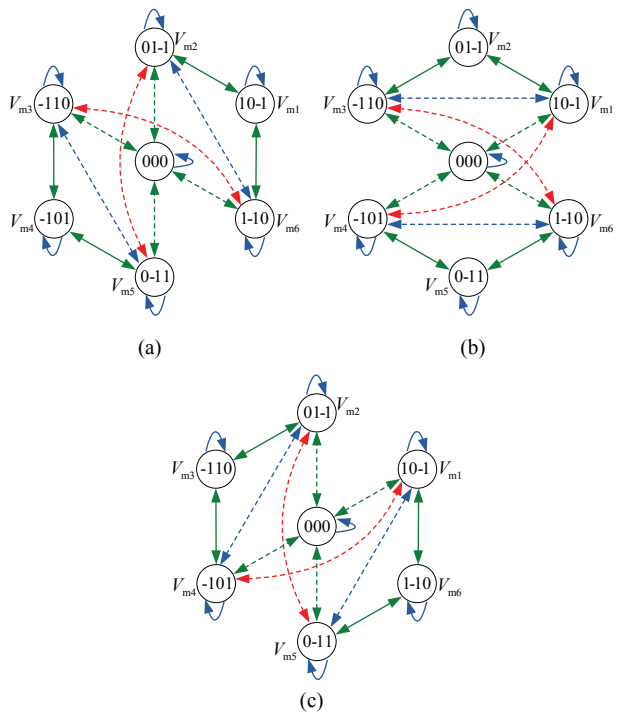

Fig. 8. Switch state graph of the proposed CMV-EL method: (a) *Sec 1* and *sec 4*, (b) *Sec 2* and *sec 5*, (c) *Sec 3* and *sec 6*.

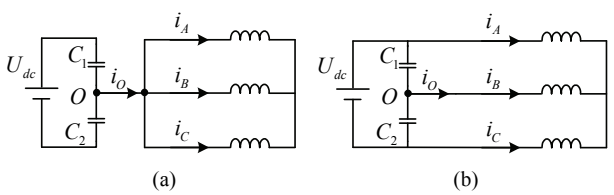

Fig. 9. The equivalent circuit of applied VVs: (a) V_0 *(000)*, (b) V_{m1} *(10−1)* .

when V_0 and V_{m1} are applied to 3LT^{2}I, respectively.

The current flow through the neutral point for all the VVs in 6MV1Z is summarized in Table V. Note that the positive current flowing through the neutral point decreases the potential of the neutral point, while the negative one has the opposite effect.

TABLE V
NP CURRENT OF DIFFERENT VVS

VVs	V_0	V_{m1}	V_{m2}	V_{m3}	V_{m4}	V_{m5}	V_{m6}
i_O	*0*	i_B	i_A	i_C	i_B	i_A	i_C

TABLE VI
SYSTEM AND CONTROL PARAMETERS

Parameters	Value
Filter inductance L	$L = 10$ *m*H
Resistance R	$R = 0.2\ \Omega$
DC-bus voltage	$U_{dc} = 100$ V
DC-bus capacitance	$C = 2$ *m*F
Line-line voltage (RMS)	$E_m = 40$ V
Fundamental frequency	$f = 50$ Hz
Dead time	$t_d = 3\ \mu s$
Control period	T_s =50/100 μs

According to Tables IV and V, the current flowing through the neutral point for the candidate VVs of the proposed CMV-EL method always includes i_A, i_B, and i_C. For a balanced three-phase system, the current of each phase satisfies $i_A + i_B + i_C = 0$, which means that among i_A, i_B, and i_C, two of them always have the opposite polarity with the third one. As previously mentioned, different polarities of the current flowing through the neutral point have different effects to the potential of the neutral point, which means that the potential of the neutral point can be controlled by the candidate VVs of the proposed CMV-EL method.

V. SIMULATION RESULTS

To confirm the aforementioned theoretical analysis and the effectiveness of the proposed CMV-EL method, a simulation model containing a 3LT^{2}I as shown in Fig. 1 was developed using MATLAB/Simulink. The system and control parameters in the simulation are fully listed in Table VI. The control period T_s is set to 100 *us* in the simulations. Fig. 10 shows the simulated waveforms obtained by the proposed CMV-EL method with the reference current of 4A. For comparison, the MPC-based 6MV1Z and conventional MPC methods for 3LT^{2}I are operated under the same conditions, and the simulated results are shown in Figs. 11 and 12.

As shown in Fig. 10(a), the grid currents of the 3LT^{2}I generated by the proposed CMV-EL method track their references accurately. However, the THD values of the grid currents of the 3LT^{2}I generated by the proposed CMV-EL method are slightly higher than those observed in the 6MV1Z and conventional MPC methods for 3LT^{2}I due to the insufficient number of VVs used for the current tracking control. Considering the different values of VVs used for the optimization, the line-to-line voltage (V_{AB}) of the 3LT^{2}I obtained by the proposed CMV-EL method shown in Fig.

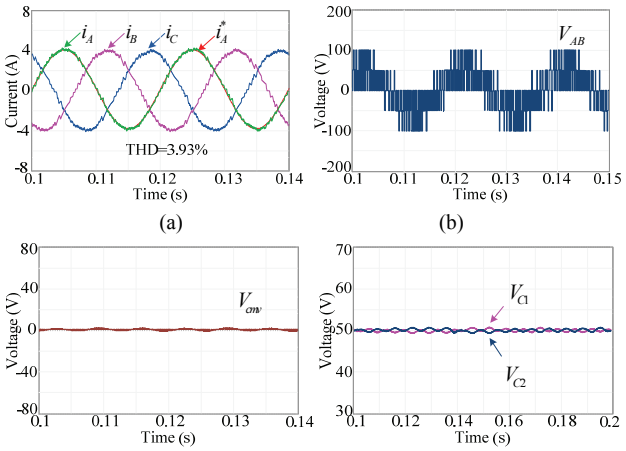

Fig. 10. Simulation waveforms of the proposed CMV-EL method: (a) The three-phase grid currents, (b) Line-to-line voltage (V_{AB}), (c) CMV, (d) Fluctuations of the NPPs.

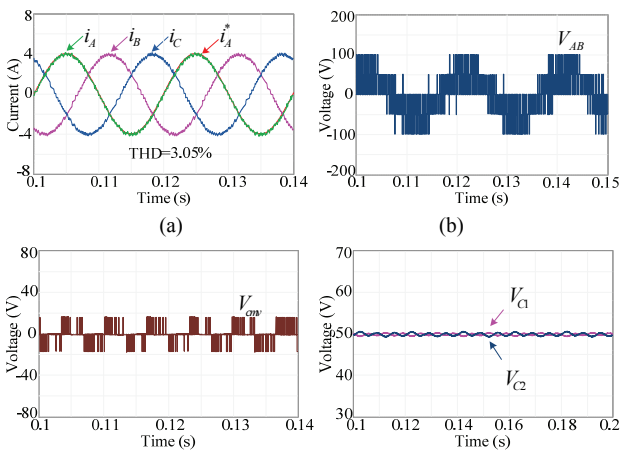

Fig. 11. Simulation waveforms of the 6MV1Z method: (a) The three-phase grid currents, (b) Line-to-line voltage (V_{AB}), (c) CMV, (d) Fluctuations of the NPPs.

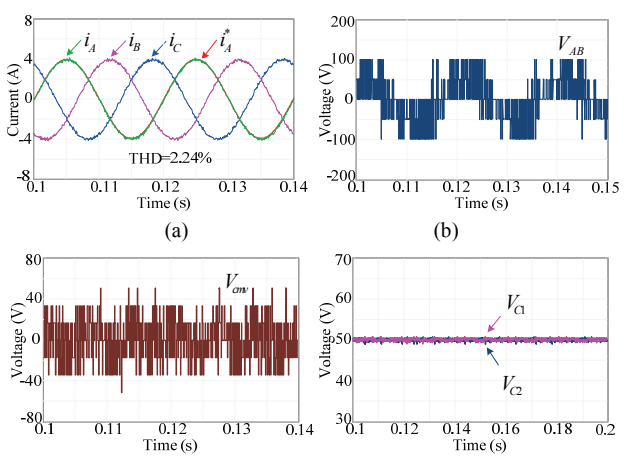

Fig. 12. Simulation waveforms of conventional MPC method: (a) The three-phase grid currents, (b) Line-to-line voltage (V_{AB}), (c) CMV, (d) Fluctuations of the NPPs.

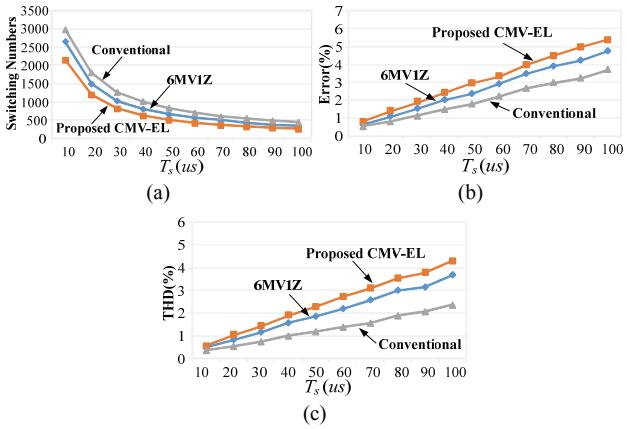

Fig. 13. Comparative results of the three methods: (a) Number of switching, (b) Current errors, (c) THD.

10(b) differs from that obtained by the 6MV1Z and conventional MPC methods for 3LT^{2}I as shown in Figs. 11(b) and 12(b), respectively. Fig. 10(c) shows that the CMV of the 3LT^{2}I has been effectively eliminated by the proposed CMV-EL method. Meanwhile, the 6MV1Z and conventional MPC methods for 3LT^{2}I generate large CMV fluctuations as shown in Figs. 11(c) and 12(c), respectively. The NPP fluctuations of the three methods presented in Figs. 10(d), 11(d), and 12(d) show that the three methods can all effectively balance the potential of the neutral point. However, the proposed CMV-EL and 6MV1Z methods generate slightly higher NPP fluctuations than the conventional MPC method for 3LT^{2}I due to insufficient number of VVs used for optimization in every control period.

Considering that the performance of the 3LT^{2}I on the basis of the MPC methods is strongly influenced by the control period, the performance of the 3LT^{2}I with the proposed CMV-EL method is compared with that of the 6MV1Z and conventional MPC methods for 3LT^{2}I in terms of the average switching numbers, current errors, and THD values of the grid currents as a function of the control period (Fig. 13). The average switching numbers are defined as the average value of the switching operation numbers of all the 12 IGBTs in a steady-state fundamental period shown as

$$n_s = \frac{1}{12}\sum_{i=1}^{4}\sum_{x=A,B,C} n_{sxi}, \tag{12}$$

where n_{sxi} represents the average switching numbers of the ith IGBT of phase x. To some extent, the average switching numbers can represent the average switching frequency of the 3LT^{2}I. The average switching numbers obtained by the three methods versus the control period are shown in Fig. 13(a). It is seen that the proposed CMV-EL method significantly decreases the average switching numbers in comparison with 6MV1Z and conventional MPC methods for 3LT^{2}I.

The percentage of the current errors is defined as the mean value of the absolute differences between the reference

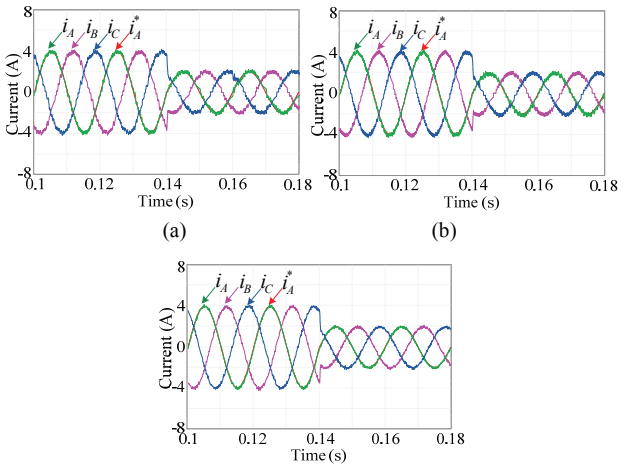

Fig. 14. Simulation waveforms of the three-phase currents with a magnitude step change from 4A to 2A with T_s = 100 *us*: (a) The proposed CMV-EL method, (b) The 6MV1Z method, (c) The conventional MPC method for 3LT^{2}I.

currents and the measured grid currents normalized to the respective RMS value of the grid current references within a given time interval of m samples [21] shown as

$$\%\text{error}(i_x) = \frac{\frac{1}{m}\sum_{x=A,B,C}\sum_{k=0}^{m}\left|i_x^*(k) - i_x(k)\right|}{\sum_{x=A,B,C}\text{rms}\left(i_x^*(k)\right)} \cdot 100\,, \tag{13}$$

where the value of m is 4000 per fundamental period. The percentage of THD is defined as

$$\%\text{THD} = \sqrt{\frac{\sum_{x=A,B,C}\sum_{h=2}^{n} i_{xh}^2}{\sum_{x=A,B,C} i_{x1}^2}} \cdot 100\,, \tag{14}$$

where i_{x1} and i_{xh} represent the fundamental and hth-harmonic components in the grid current of phase x, respectively. The number h was set to 6500 in the simulations. The results of the percentage of the grid errors and the THD values for the three methods are shown in Fig. 13(b) and (c), respectively. The proposed CMV-EL method exhibits higher grid current errors and THD values than the 6MV1Z and conventional MPC methods for 3LT^{2}I because of less candidate VVs used for the current control in every control period. However, considering that the computational burden of the proposed CMV-EL method is significantly reduced, the same grid current errors and the THD performance of the grid currents can be easily achieved in practical applications by simply decreasing the control period according to the results shown in Fig. 13.

Fig. 14 presents the simulation results obtained by the three methods with a half-step change in magnitude of the reference current. The three-phase grid currents generated by the proposed CMV-EL method can follow the reference change in magnitude as fast as the 6MV1Z and conventional MPC methods for 3LT^{2}I.

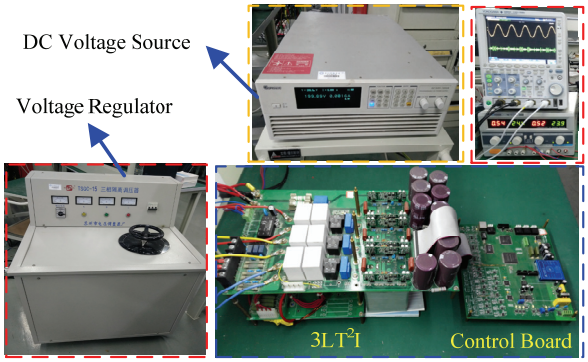

Fig. 15. Photograph of the experimental setup.

VI. Experimental Results

In this section, experiments were conducted on a prototype as shown in Fig. 15, where the entire algorithms of the proposed CMV-EL method were implemented on a DSP chip TMS320F28335. The parameters for the 3LT^{2}I and control in the experiments are the same as those in the simulations as listed in Table VI. Fig. 16 presents the experimental results obtained by the proposed CMV-EL method with T_s = 100 *us*. For comparison, 6MV1Z and conventional MPC methods for 3LT^{2}I are operated under the same operating conditions, and the experimental results are shown in Figs. 17 and 18. The control period T_s was set to 100 *us* in the experimental studies because the execution time required to complete the entire algorithm of the conventional MPC method for 3LT^{2}I reaches 61.09 *us*. However, the 6MV1Z and proposed CMV-EL methods significantly reduced the execution time to 32.47 and 27.56 (29.61) *us*, respectively. The computational burden of the digital processor is significantly reduced for the proposed CMV-EL method compared with the 6MV1Z and conventional MPC methods. Thus, a smaller control period can be easily achieved by the proposed CMV-EL method.

The experimental results shown in Figs. 16, 17, and 18 are similar to those in simulation results shown in Figs. 10, 11, and 12. The grid currents generated by the three methods can track their references accurately. However, the proposed CMV-EL method generated higher grid current THD values due to the insufficient number of VVs used for the current control. Note that the THD values are obtained by using the power analysis application module in the YOKOGAWA digital oscilloscope (350MHz DLM2034). The output voltage of the 3LT^{2}I obtained by the proposed CMV-EL method in Fig. 16(b) differs from that of the 6MV1Z and conventional MPC methods for 3LT^{2}I in Figs. 17(b) and 18(b) because of different candidate VVs used for the optimization in every control period. However, less CMV fluctuations are generated by the proposed CMV-EL method as shown in Fig. 16(c) compared with the simulation results in Fig. 10(c) because of the polarity misjudgment of the grid currents during the zero crossing in the experimental study. However,

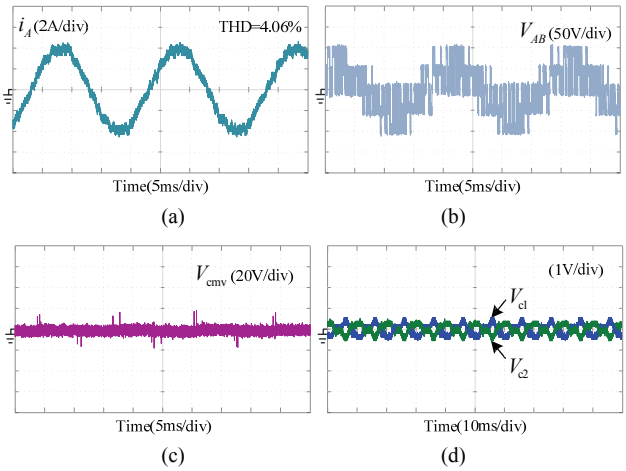

Fig. 16. Experimental waveforms of the proposed CMV-EL method: (a) Grid current i_A, (b) Line-to-line voltage (V_{AB}), (c) CMV, (d) Fluctuations of the NPPs.

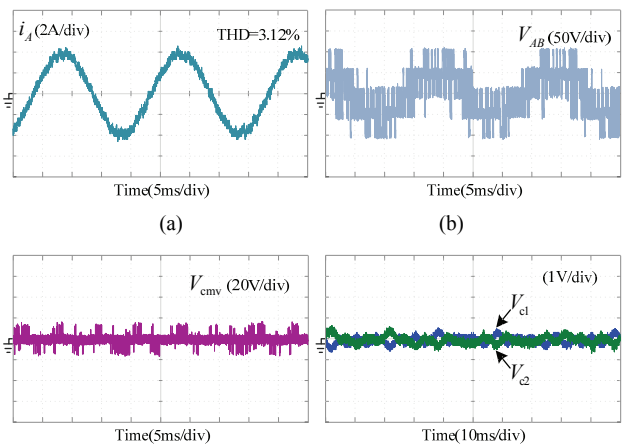

Fig. 17. Experimental waveforms of the 6MV1Z method: (a) Grid current i_A, (b) Line-to-line voltage (V_{AB}), (c) CMV, (d) Fluctuations of the NPPs.

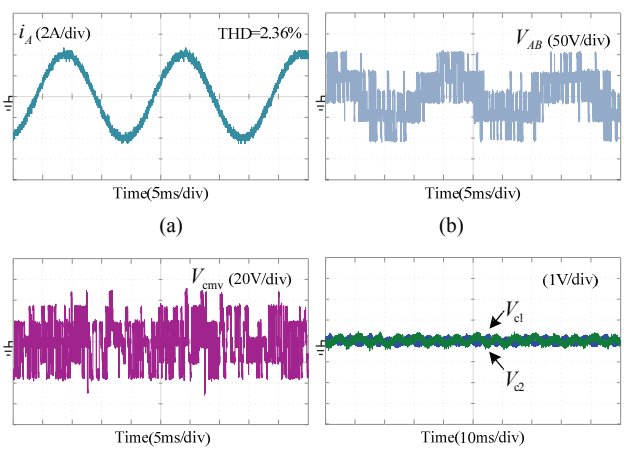

Fig. 18. Experimental waveforms of the conventional MPC method: (a) Grid current i_A, (b) Line-to-line voltage (V_{AB}), (c) CMV, (d) Fluctuations of the NPPs.

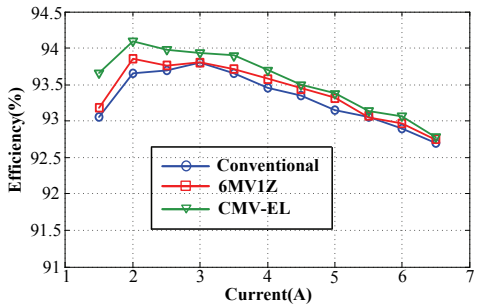

Fig. 19. Experimental efficiency waveforms.

TABLE VII
COMPARISON RESULTS FOR THE THREE METHODS

Method	CMV-EL	6MV1Z	Con_MPC
CMV	Constant	Constant	Variable
Max v_{xn}	$U_{dc}/2$	$U_{dc}/3$	$U_{dc}/\sqrt{3}$
NPP fluctuations	Low	Low	Low
Efficiency	High	Medium	Low
THD	High	Medium	Low
Switching numbers	Low	Medium	High
Calculation time	27.56 or 29.61 *us*	32.47 *us*	61.09 *us*

both the peak value and the fluctuation times of the CMV are significantly reduced compared with those of the 6MV1Z and conventional MPC methods for 3LT^{2}I as shown in Figs. 17(c) and 18(c), respectively. The experimental waveforms of the NPP fluctuations of the three methods presented in Figs. 16(d), 17(d), and 18(d) show that the NPP fluctuations obtained by the three methods are within 1 V, and the proposed CMV-EL and 6MV1Z methods generate slightly higher NPP fluctuations than the conventional MPC method for 3LT^{2}I, which is consistent with the results in simulations.

Experimental efficiency values of the three methods are directly obtained by the power analyzer (WT1800 of YOKOGAWA) with the parameters shown in Table VI, where the results are shown in Fig. 19. As expected, the proposed CMV-EL method exhibits the best efficiency performance among the three methods because it achieves the lowest overall switching numbers.

For a more intuitive understanding of the advantages and drawbacks of each method, comprehensive comparisons of the three methods with the parameters shown in Table VI are summarized in Table VII.

Considering that the proposed CMV-EL method can achieve a smaller control period, the experimental waveforms obtained by the proposed CMV-EL method with T_s = 50 μs are shown in Fig. 20. It is observed that the grid current generated by the proposed CMV-EL method can achieve the same current errors and THD performance with the conventional MPC method for 3LT^{2}I (100 *us*) without significantly increasing the average switching numbers according to the analysis results shown in Fig. 13. Thus, although utilizing

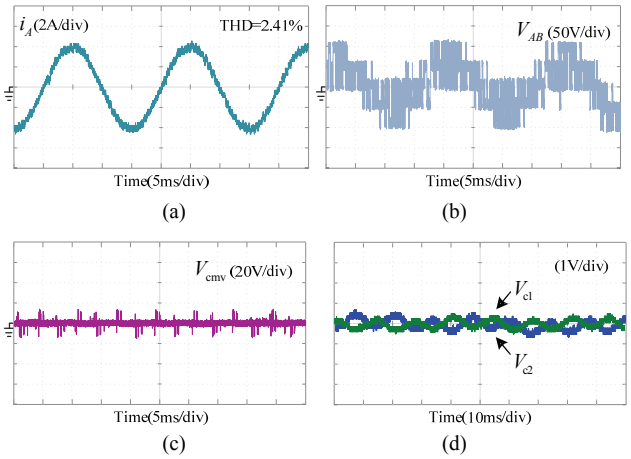

Fig. 20. Experimental waveforms of the proposed CMV-EL with T_s = 50 μs: (a) Grid currents i_A, (b) Line-to-line voltage (V_{AB}), (c) CMV, (d) Fluctuations of the NPP.

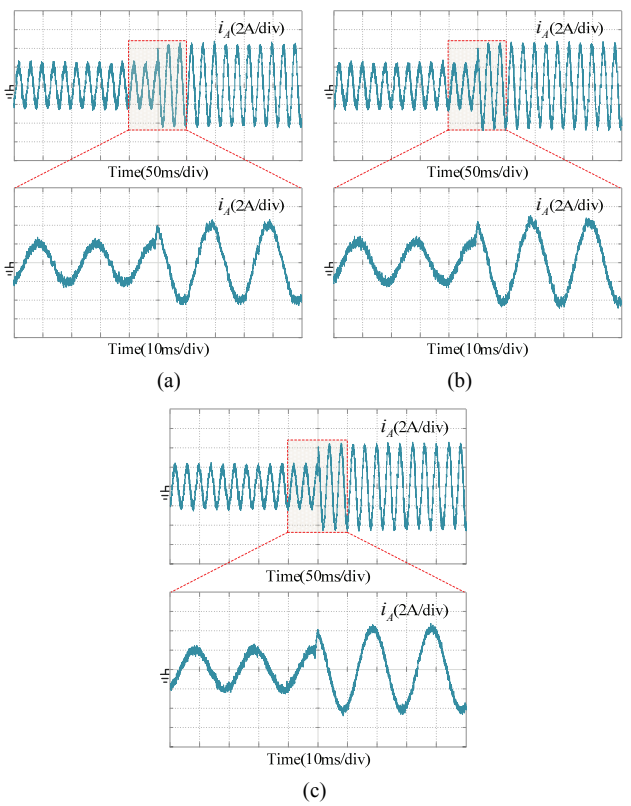

Fig. 21. Experimental waveforms of the phase current with a magnitude step change from 2A to 4A with T_s = 100 μs: (a) Proposed CMV-EL method, (b) 6MV1Z method, (c) conventional MPC method.

less candidate VVs in the proposed CMV-EL method to eliminate the CMV may deteriorate the performance of the grid currents, this approach reduced the complexity of calculation, and the same current errors and THD performances with the conventional MPC method for 3LT^{2}I can be achieved by simply decreasing the control period.

Fig. 21 shows the experimental results of the dynamic responses obtained by the three methods with the control period T_s = 100 μs. The grid currents generated by the proposed CMV-EL method can follow the magnitude step changes of the reference with fast dynamics as observed in the 6MV1Z and conventional MPC methods.

VII. Conclusion

This study proposes a new MPC-based CMV-EL method for 3LT^{2}Is with dead-time effects taken into account. The candidate VVs of the proposed CMV-EL method are redesigned by pre-excluding the VVs that will cause CMV fluctuations during the dead time. The proposed CMV-EL method can effectively eliminate the CMV as well as control the grid current and balance the NPPs. Simulation and experimental results show that the proposed CMV-EL method can reach satisfactory performances in both steady and dynamic states. Furthermore, both the computational burden and the average switching numbers are reduced at the cost of higher current errors and THD values. However, because of a shorter execution time needed in the practical application, the proposed CMV-EL method can achieve the same current errors and THD performance with the conventional MPC method by simply decreasing the control period.

Acknowledgment

This work was supported by the National Natural Science Foundation of China (No. 51707030).

References

[1] A. Nabae, I. Takahashi, and H. Akagi, "A new neutral-point-clamped PWM inverter," *IEEE Trans. Ind Appl.*, Vol. IA-17, No. 5, pp. 518–523, Sep./Oct. 1981.

[2] M. Schweizer and J. W. Kolar, "Design and implementation of a highly efficient three-level T-type converter for low-voltage applications," *IEEE Trans. Power Electron.*, Vol. 28, No. 2, pp. 899-907, Feb. 2013.

[3] U. M. Choi, F. Blaabjerg, and K. B. Lee, "Reliability improvement of a T-Type three-level inverter with fault-tolerant control strategy," *IEEE Trans. Power Electron.*, Vol. 30, No. 5, pp. 2660-2673, May 2015.

[4] R. Teichmann and S. Bernet, "A comparison of three-level converters versus two-level converters for low-voltage drives traction and utility applications," *IEEE Trans. Ind. Appl.*, Vol. 41, No. 3, pp. 855-865, May/Jun. 2005.

[5] Y. Atia and M. Salem, "Microcontroller-based improved predictive current controlled VSI for single-phase grid-connected systems," *J. Power Electron.*, Vol. 13, No. 6, pp. 1016–1023, Nov. 2013.

[6] M. P. Kazmierkowski, R. Krishnan, and F. Blaabjerg, *Control in Power Electronics*. New York, NY, USA: Academic, 2002.

[7] C. Xie, X. Zhao, K. Li, J. Zou, and J. M. Guerrero, "A new tuning method of multi-resonant current controllers for grid-connected voltage source converters," *IEEE J. Emerg.*

Sel. Top. Power Electron., to be published. DOI: 10.1109/JESTPE.2018.2833806

[8] J. M. Erdman, R. J. Kerkman, D. W. Schlegel, and G. L. Skibinski, "Effect of PWM inverters on AC motor bearing currents and shaft voltages," *IEEE Trans. Ind. Appl*., Vol. 32, No. 2, pp. 250-259, Feb. 1996.

[9] J. D. Barros, J. F. A. Silva, and É. G. A. Jesus, "Fast-predictive optimal control of NPC multilevel converters," *IEEE Trans. Ind. Electron*., Vol. 60, No. 2, pp. 619-627, Feb. 2013.

[10] S. Kwak and J. C. Park, "Predictive control method with future zero-sequence voltage to reduce switching losses in Three-Phase voltage source inverters," *IEEE Trans. Power Electron*., Vol. 30, No. 3, pp. 1558-1566, Mar. 2015.

[11] J. Rodríguez, J. Pontt, C. A. Silva, P. Correa, P. Lezana, P. Cortés, and U. Ammann, "Switching strategy based on model predictive control of VSI to obtain high efficiency and balanced loss distribution," *IEEE Trans. Power Electron*., Vol. 29, No. 9, pp. 4551-4567, Sep. 2014.

[12] J. M. Erdman, R. J. Kerkman, D. W. Schlegel, and G. L. Skibinski, "Effect of PWM inverters on AC motor bearing currents and shaft voltages," *IEEE Trans. Ind. Appl*., Vol. 32, No. 2, pp. 250-259, Mar./Apr. 1996.

[13] M. J. Duran, J. A. Riveros, F. Barrero, H. Guzman, and J. Prieto, "Reduction of common-mode voltage in five-phase induction motor drives using predictive control techniques," *IEEE Trans. Ind Appl.*, Vol. 48, No. 6, pp. 2059-2067, Nov./Dec. 2012.

[14] M. C. Cavalcanti, A. M. Farias, K. C. Oliveira, F. A. S. Neves, and J. L. Afonso, "Eliminating leakage currents in neutral point clamped inverters for photovoltaic systems," *IEEE Trans. Ind. Electron.*, Vol. 59, No. 1, pp. 435-443, Jan. 2012.

[15] X. Wang, J. Zou, L. Ma, J. Zhao, C. Xie, K. Li, L. Meng, and J. M. Guerrero, "Model predictive control methods of leakage current elimination for a three-level T-type transformerless PV inverter," *IET Power Electron.*, Vol. 11, No. 8, pp. 1492-1498, Jul. 2018.

[16] R. M. Tallam, R. J. Kerkman, D. Leggate, and R. A. Lukaszewski, "Common-mode voltage reduction PWM method for AC Drives," *IEEE Trans. Ind. Appl*., Vol. 46, No. 5, pp. 1959-1969, Sep./Oct. 2010.

[17] J. W. Kimball and M. Zawodniok, "Reducing common-mode voltage in three-phase sine-triangle PWM with interleaved carriers," *IEEE Trans. Power Electron*., Vol. 26, No. 8, pp. 2229-2236, Aug. 2011.

[18] M. C. Cavalcanti, K. C. de Oliveira, A. M. de Farias, F. A. S. Neves, G. M. S. Azevedo, and F. C. Camboim, "Modulation techniques to eliminate leakage currents in transformerless three-phase photovoltaic systems," *IEEE Trans. Ind. Electron.*, Vol. 57, No. 4, pp. 1360-1368, Apr. 2010.

[19] X. Wu, G. Tan, Z. Ye, Y. Liu, and S. Xu, "Optimized common-mode voltage reduction PWM for three-phase voltage source inverters," *IEEE Trans. Power Electron.*, Vol. 31, No. 4, pp. 2959-2969, Apr. 2016.

[20] L. Kai, J. Zhao, W. Wu, M. Li, L. Ma, and G. Zhang, "Performance analysis of zero common-mode voltage pulse-width modulation techniques for three-level neutral point clamped inverters," *IET Power Electron.*, Vol. 9, No. 14, pp. 2654-2664, Nov. 2016.

[21] S. Mun and S. Kwak, "Reducing common-mode voltage of three-phase VSIs using the predictive current control method based on reference voltage," *J. Power Electron*., Vol. 15, No. 3, pp. 712-720, May 2015.

[22] S. Kwak and S. Mun, "Model predictive control methods to reduce common-mode voltage for three-phase voltage source inverters," *IEEE Trans. Power Electron*., Vol. 30, No. 9, pp. 5019-5035, Sep. 2015.

[23] S. Kwak and J. Park, "Model predictive direct power control with vector preselection technique for highly efficient active rectifiers," *IEEE Trans. Ind. Informat*, Vol. 11, No. 1, pp. 44-52, Feb. 2015.

[24] L. Guo, X. Zhang, S. Yang, Z. Xie, and R. Cao, "A model predictive control-based common-mode voltage suppression strategy for voltage-source inverter," *IEEE Trans. Ind. Electron.*, Vol. 63, No. 10, pp. 6115-6125, Oct. 2016.

[25] S. Kwak and S. Mun, "Common-mode voltage mitigation with a predictive control method considering dead time effects of three-phase voltage source inverters," *IET Power Electron.*, Vol. 8, No. 9, pp. 1690-1700, Sep. 2015.

[26] X. Xing, A. Chen, Z. Zhang, J. Chen, and C. Zhang, "Model predictive control method to reduce common-mode voltage and balance the neutral-point voltage in three-level T-type inverter," *2016 IEEE Applied Power Electronics Conference and Exposition (APEC)*, pp. 3453-3458, 2016.

[27] E. A. Kumar, K. C. Sekhar, and R. S. Rao, "Model predictive current control of a three-phase T-type NPC inverter to reduce common mode voltage," *J. Circuits, Syst. Comp.*, Vol. 27, No. 2, Feb. 2018.

[28] X. Wang, J. Zou, J. Zhao, Z. Dong, M. Wei, C. Xie, and K. Li, "Common-mode voltage elimination of three-level T-type inverters with a finite control set model predictive control method," *2018 IEEE Applied Power Electronics Conference and Exposition (APEC)*, pp. 992-997, 2018.

[29] S. Kouro, P. Cortes, R. Vargas, U. Ammann, and J. Rodriguez, "Model predictive control – A simple and powerful method to control power converters," *IEEE Trans. Ind. Electron*., Vol. 56, No. 6, pp. 1826-1838, Jun. 2009.

[30] P. Cortes, J. Rodriguez, C. Silva, and A. Flores, "Delay compensation in model predictive current control of a three-phase inverter," *IEEE Trans. Ind. Electron.*, Vol. 59, No. 2, pp. 1323-1325, Feb. 2012.

Xiaodong Wang was born in SiChuan, China in 1989. He obtained his M.S. in Control Theory and Control Engineering from the University of Electronic Science and Technology of China, Chengdu, China in 2015, where he has been working for a Ph.D. since 2016. His current research interests include distributed renewable power generation, microgrids, model predictive control of multilevel inverters, and voltage source inverters.

Jianxiao Zou received the B.S., M.S., and Ph.D. degrees in control science and engineering from the University of Electronic Science and Technology of China, Chengdu, China in 2000, 2003, and 2009, respectively. He is currently a professor at the University of Electronic Science and Technology of China (UESTC). He served as the vice dean of the School of Automation Engineering in 2011. He also served as the vice president of the Sichuan Electrotechnical Society, vice president of the Society for electrical engineering, and the chairman of the member development, Chengdu Section of IEEE China. He was a visiting scholar at the University of California, Berkeley (UC Berkeley) in 2010 and a senior visiting professor of Rutgers, The State University of New Jersey in 2014. His research interests include control theory and control engineering, renewable energy control technologies, and intelligent information processing and control. He organized more than 10 international conferences/symposiums, wherein he was the general/program chair and session chair. He has published more than 50 journal papers and has been authorized more than 120 national invention patents.

Zhenhua Dong obtained his B.S in Automation from the University of Electronic Science and Technology of China, Chengdu, China in 2011, where he has been working for an M.S. since 2015. His research interests include new energy and current control for distributed systems.

Chuan Xie received his B.S. degree in automation engineering from the University of Electronic Science and Technology of China, Chengdu, China and the Ph.D. degree in power electronics from Zhejiang University, Hangzhou, China in 2007 and 2012, respectively. Since 2012, he was a lecturer in the School of Automation Engineering at the University of Electronic Science and Technology of China. From May 2015 to 2016, he was a visiting scholar at the Department of Energy Technology, Aalborg University. His main research interests include digital control of power electronics, grid synchronization technology, distributed generation systems, microgrids, and power quality.

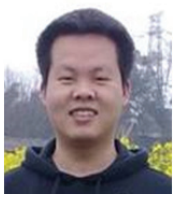

Kai Li was born in 1983. He obtained his B.S., M.S., and Ph.D. in Automation Engineering from the University of Electronic Science and Technology of China, Chengdu, China in 2006, 2009, and 2014, respectively. He is currently working as an associate professor in the University of Electronic Science and Technology of China. His current research interests include multilevel inverters, storage converters, and microgrids.

Josep M. Guerrero obtained his B.S. in Telecommunications Engineering, M.S. in Electronics Engineering and Ph.D. in Power Electronics from the Technical University of Catalonia, Barcelona, in 1997, 2000, and 2003, respectively. He has been a full-time professor in the Department of Energy Technology, Aalborg University, Denmark since 2011. His research interests is oriented toward different microgrid aspects, including power electronics, distributed energy storage systems, hierarchical and cooperative control, energy management systems, smart metering, and the Internet of things for AC/DC microgrid clusters and islanded minigrids. Recently, he particularly focuses on maritime microgrids for electrical ships, vessels, ferries, and seaports.